

Symmetry energy: nuclear masses and neutron stars

J. M. Pearson¹, N. Chamel², A. F. Fantina², and S. Goriely²

¹ Dépt. de Physique, Université de Montréal, Montréal (Québec), H3C 3J7 Canada

² Institut d'Astronomie et d'Astrophysique, CP-226, Université Libre de Bruxelles, 1050 Brussels, Belgium

Received: date / Revised version: date

Abstract. We describe the main features of our most recent Hartree-Fock-Bogoliubov nuclear mass models, based on 16-parameter generalized Skyrme forces. They have been fitted to the data of the 2012 Atomic Mass Evaluation, and favour a value of 30 MeV for the symmetry coefficient J , the corresponding root-mean square deviation being 0.549 MeV. We find that this conclusion is compatible with measurements of neutron-skin thickness. By constraining the underlying interactions to fit various equations of state of neutron matter calculated *ab initio* our models are well adapted to a realistic and unified treatment of all regions of neutron stars. We use our models to calculate the composition, the equation of state, the mass-radius relation and the maximum mass. Comparison with observations of neutron stars again favours a value of $J = 30$ MeV.

PACS. 21.65.Ef Symmetry energy – 21.10.Dr Binding energies and masses – 97.60.Jd Neutron stars – 21.60.Jz Nuclear Density Functional Theory and extensions – 26.60.Kp Equations of state of neutron-star matter

1 Introduction

The concept of nuclear symmetry energy probably arises most naturally in connection with the liquid-drop model of the nucleus, which was inspired in large part by the observation that the sharp radius R of any nucleus with Z protons and N neutrons is given by $R \simeq r_0 A^{1/3}$, where the mass number $A = N + Z$ and r_0 is a constant. The roughly constant density is what one would expect in view of the saturated character of nuclear forces, i.e., their finite range and strong short-range repulsion, and suggests in the first instance that nuclei consist simply of differently sized pieces of a homogeneous substance, “nuclear matter”. In this extreme picture the internal energy e per nucleon would be the same for all nuclei, but the liquid-drip model takes into account surface tension, the non-saturating character of the Coulomb force and a “composition” dependence, writing

$$e = a_v + JI^2 + (a_{sf} + a_{ss}I^2) A^{-1/3} + \frac{3e^2}{5r_0} Z^2 A^{-4/3}. \quad (1)$$

With $I = (N - Z)/A$, this expression admits so-called volume-symmetry and surface-symmetry terms; the dominant contribution to both the kinetic-energy and potential-energy parts of these terms comes from the Pauli principle, although the spin dependence and finite range of the nuclear forces play a role also. Fitting the five parameters of Eq. (1) to the data of the 2012 Atomic Mass Evaluation (AME) [1], we find: $a_v = -15.65$ MeV, $J = 27.30$ MeV, $a_{sf} = 17.58$ MeV, $a_{ss} = -24.16$ MeV and $r_0 = 1.230$ fm;

the root-mean square (rms) deviation of this fit to 2353 nuclei is 3.03 MeV.

It is the sum of the first two terms of the right-hand side of Eq. (1), $a_v + JI^2$, that represents, in the absence of any Coulomb effects, the energy per nucleon of homogeneous or infinite nuclear matter, the density of which is $n_0 = 3/(4\pi r_0^3)$, i.e., around 0.16 nucleons per cubic fermis. However, if we let A become very big while keeping I , and hence Z/A , constant Eq. (1) goes over into

$$e = a_v + JI^2 + \frac{3e^2}{20r_0} (1 - I)^2 A^{2/3}, \quad (2)$$

which means that the energy per nucleon diverges in this limit, because of the Coulomb term. In a purely neutronic system, $I = 1$, the Coulomb term vanishes, but then in view of the above empirical values of the drop-model parameters the energy per nucleon, $e = a_v + J$, is positive, i.e., the system is unbound. Thus it appears that because of the joint action of the Coulomb term and volume-symmetry term it is impossible to have a piece of nuclear matter large enough for all but the volume terms in the energy to be negligible.

However, let us put gravity into the drop-model expression (2) [2]. Since this, although attractive, has the same non-saturating character as the Coulomb force, Eq. (2) is replaced by

$$e = a_v + JI^2 + \frac{3}{5r_0} \left\{ \frac{e^2}{4} (1 - I)^2 - GM^2 \right\} A^{2/3}, \quad (3)$$

where G is the gravitational constant and M the nucleon mass. As long as protons are present, i.e., $I < 1$, the Coulomb term will totally overwhelm the gravitational term and the system will be unbound. But using the above values of the parameters we find that a purely neutronic system will be gravitationally bound for $A > 3.4 \times 10^{56}$, i.e., for a mass in excess of 5.6×10^{29} kg, which is within an order of magnitude of the mass of a typical neutron star. Furthermore, the nuclear density n_0 is within an order of magnitude that of neutron stars, typical radii being around 10 km.

This picture of a neutron star as a single giant nucleus, bound not by nuclear forces but by gravity is, of course, grossly oversimplified. In the first place, the star does not consist entirely of neutrons, but rather of a neutral mixture of neutrons, protons and leptons (electrons and muons) in beta equilibrium. Secondly, while the bulk of the star is indeed homogeneous the density is by no means constant, falling steadily from several times the nuclear density n_0 at the centre to zero at the surface. Moreover, the equation of hydrostatic equilibrium that the density variations must satisfy can only be formulated within the framework of general relativity, one consequence of which is that there is an upper limit on the gravitational mass of neutron stars. (However, the fact that there is also a *lower* limit can be understood qualitatively by reference to Eq. (3): if the mass of the star falls below a certain value it is blown apart by the symmetry energy.)

Actually, when the density falls below about $n_0/2$ the homogeneous medium breaks up into inhomogeneities. This marks the transition from the core to the crust of the star (see, e.g., Ref. [3] for a review). The inner part of the crust consists of neutron-proton clusters along with free neutrons and electrons, while the outer part, below a density of about 2.6×10^{-4} nucleons per cubic fermis, consists of just bound nuclei and electrons, with no free neutrons remaining. The nuclei found in this region will generally be highly neutron rich, and those at the interface will be on the neutron drip line. As the surface is approached the nuclei become less and less neutron rich, and at the surface of the star only nuclei that are stable under natural terrestrial conditions are found.

However, all but a tiny fraction of the nucleons of a neutron star are located in its core, which means that global properties such as the maximum possible mass are determined essentially by the properties of homogeneous beta-equilibrated nuclear matter, which we refer to as neutron-star matter. To discuss these latter properties it is convenient to begin by neglecting the presence of electrons and muons, even though they play a crucial role (it is trivially easy to take account of them), and simply generalize to arbitrary density the notion of the hypothetical Coulomb-free infinite nuclear matter (INM) introduced in connection with the first two terms of the liquid-drop expression (1). For INM of proton density n_p and neutron density n_n we write the equation of state (EoS) i.e., the energy per nucleon as a function of the total density $n = n_p + n_n$ and charge asymmetry $\eta = (n_n - n_p)/n$ (throughout this paper we assume zero temperature), in

the form

$$e(n, \eta) = e(n, \eta = 0) + S_1(n)\eta^2 + O(\eta^4) \quad , \quad (4)$$

in which the first term on the right-hand side is just the energy per nucleon of charge-symmetric INM. Identifying n_0 as the equilibrium density of charge-symmetric INM, we then expand $e(n, \eta = 0)$ and the symmetry energy $S_1(n)$ about n_0 in powers of $\epsilon = (n - n_0)/n_0$, thus

$$e(n, \eta = 0) = a_v + \frac{1}{18}K_v\epsilon^2 - \frac{1}{162}K'\epsilon^3 + \dots \quad (5a)$$

and

$$S_1(n) = J + \frac{1}{3}L\epsilon + \frac{1}{18}K_{sym}\epsilon^2 + \dots \quad (5b)$$

Of particular interest in the context of neutron stars is the special case of $\eta = 1$, i.e., pure neutron matter (NeuM), the energy per neutron of which we write as

$$e(n, \eta = 1) = e(n, \eta = 0) + S_2(n) \quad . \quad (6)$$

Both $S_1(n)$ and $S_2(n)$ have been generally referred to as the ‘‘symmetry energy’’, but, because of the terms $O(\eta^4)$ in Eq. (4), these two functions are not identical. Actually, at nuclear densities the difference is very small but it can become significant at higher densities (see, for example, Section III of Ref. [4]); in any case, it would be more appropriate to speak of ‘‘asymmetry energy’’.

A crucial quantity in discussing the internal hydrostatic equilibrium in neutron stars is the pressure, given in homogeneous INM by $P = n^2 \{\partial e(n, \eta)/\partial n\}_\eta$ (in actual neutron-star matter the lepton pressure has to be added to this). For n close to n_0 in NeuM this reduces to $P = Ln_0/3$, whence the importance that has been attached to the L parameter. However, in the more general case the pressure depends not only on the symmetry energy (of either kind) but also on the energy per nucleon of charge-symmetric INM, $e(n, \eta = 0)$. Thus we shall be concerned here not just with symmetry energy but with charge-asymmetric INM in general.

Laboratory experiments provide us with considerable, but by no means complete, information on the EoS of INM up to a density of around 4 or $5n_0$ (see, e.g., Ref. [5] for a recent review of different methods, and Section II of this volume). In this paper it is nuclear masses that provide the principal source of laboratory data on which we will draw, although we will also examine the implications of neutron-skin measurements.

But in the heavier neutron stars the core density can reach $10n_0$, and information on the EoS at such high densities can only be obtained through *ab initio* many-body calculations of INM starting from realistic nucleonic interactions, as determined by nucleon-nucleon scattering and the bound states of two- and three-nucleon systems, with possibly some guidance from meson-exchange theory or QCD (see, e.g., Section I of this volume). In principle, these calculations should be performed as a function

of both density n and asymmetry η , although it should be noted that the calculations are more reliable for the case $\eta = 1$, i.e., pure NeuM, for the following reasons: i) two-nucleon scattering determines the phase parameters better in the $T = 1$ than in the $T = 0$ states; ii) the strongly tensor-coupled 3S_1 and 3D_1 states are absent; iii) the relatively poorly determined three-nucleon force is less important in this case (it would not contribute at all to NeuM if it had zero range).

Besides homogeneous INM, *ab initio* calculations of this kind have been carried out only for light nuclei and a few medium-mass nuclei, and thus cannot be used for either the inner or outer crusts. However, for the EoS of the outer crust all that is required are the masses of the appropriate nuclei, and for the outermost layers these are known experimentally, namely [6, 7]: ${}^{56}\text{Fe}$, ${}^{62}\text{Ni}$, ${}^{64}\text{Ni}$, ${}^{66}\text{Ni}$, ${}^{86}\text{Kr}$, ${}^{84}\text{Se}$, ${}^{82}\text{Ge}$ and ${}^{80}\text{Zn}$. For the more neutron-rich nuclei of the deeper layers of the outer crust recourse must be made to theoretical mass tables, whose extrapolations from the data may be expected to be more reliable the more they are microscopically based. The most microscopic atomic mass models currently available are based on the Hartree-Fock-Bogoliubov (HFB) method with effective interactions of the Skyrme or Gogny type. The rms deviations of the most accurate models lie below 0.6 MeV [4]. As mass measurements are pushed ever closer to the neutron drip line we can expect that at some time in the future the masses of all the nuclei found in the outer crust will have been measured, making the use of theoretical mass models in this region unnecessary [8].

On the other hand, the inhomogeneous nuclear matter found in the inner crust of a neutron star cannot be reproduced in the laboratory, and the resort to theory is inevitable. Since the seminal work of Negele and Vautherin [9] mean-field calculations have been generally performed within the Wigner-Seitz framework [10,11]: the crust is replaced by a set of independent spherical cells each of which contains only one cluster. However this approach can only be reliably applied in the shallowest layers of the inner crust because of the appearance of spurious neutron quantum shell effects [12]. These effects persist in calculations using a cubic cell with periodic boundary conditions [13,14,15], and can only be properly eliminated by using the band theory of solids [12]. However, the calculations would then become computationally prohibitive. In previous papers on the inner crust [16,17] we have adopted the simpler approach of neglecting entirely neutron shell effects, and applying the semi-classical extended Thomas-Fermi method. Proton shell effects, which, unlike neutron shell effects, are generally not negligible, are easily taken into account via the Strutinsky integral theorem. This method is extended in the present paper to include pairing correlations, treated within the BCS approximation as discussed in Ref. [18]. While still limited to spherical symmetry this restriction is not expected to have a significant impact on the calculated EoS.

Effective interactions used in the outer and inner parts of the crust can also provide a convenient parametrization of the EoS of INM, as obtained from realistic cal-

culations. In this way, it is possible to construct unified EoSs of neutron stars ensuring a thermodynamically consistent treatment of the transitions between the different regions of the star. Such a treatment is of particular importance for avoiding the occurrence of spurious instabilities in neutron-star dynamical simulations. For this reason, unified EoSs are well suited for neutron-star modelling. In turn, by comparing these models to astrophysical observations, one can extract valuable information on the EoS of INM (see, e.g., Ref. [19] for a recent review; see also Section III of this volume).

We describe our recent HFB models in Section 2, showing how they can be used to extract the symmetry coefficient J from the mass data. In Section 3 we apply these models to a unified treatment of neutron stars, calculating in particular the composition and the mass-radius relation, with an assessment of the impact of the symmetry energy. Our conclusions are summarized in Section 4.

2 The Skyrme-Hartree-Fock-Bogoliubov mass models

Our HFB mass models are intended to facilitate the reliable extrapolation of nuclear-mass data out to the highly neutron-rich environments of astrophysical interest, such as neutron stars and the gravitationally collapsing cores of supernovae. As such, they are well adapted to the extraction of information on symmetry energy from both nuclear data and the observation of neutron stars. They likewise enable us to investigate the implications of our (incomplete) knowledge of symmetry energy for the properties of neutron stars and supernova cores.

In this paper we shall refer only to our latest mass models, HFB-19 to HFB-26, along with their underlying density functionals, BSk19 to BSk26, respectively [4, 20]. All are based on the 16-parameter generalized form of Skyrme force given in Eq. (1) of Ref. [4], the unconventional feature of which is the appearance of so-called t_4 and t_5 terms, density-dependent generalizations of the usual t_1 and t_2 terms, respectively. The full formalism for this generalized Skyrme force is presented in the Appendix of Ref. [21], but note that we now drop all the terms quadratic in the spin-current tensor and their time-odd counterpart from the Hamiltonian density, for the reasons explained in Ref. [22]. The parameters of this form of force were determined primarily by fitting measured nuclear masses, which were calculated with the HFB method. For this it was necessary to supplement the Skyrme forces with a microscopic pairing force (5 parameters), phenomenological Wigner terms (4 parameters) and correction terms for the spurious collective energy (5 parameters).

However, with a view to enhancing the reliability of the extrapolations to all parts of neutron stars, and to other neutron-rich systems as well, in fitting the mass data we simultaneously constrained the Skyrme force to fit the zero-temperature EoS of homogeneous neutron matter (NeuM), as determined by many-body calculations with realistic two- and three-nucleon forces. Actually, several

Table 1. Maximum neutron-star mass \mathcal{M}_{max} (in units of the mass of the Sun \mathcal{M}_\odot) for different models.

Force	$\mathcal{M}_{max}/\mathcal{M}_\odot$
BSk19	1.86
BSk20	2.15
BSk21	2.28
BSk22	2.26
BSk23	2.27
BSk24	2.28
BSk25	2.22
BSk26	2.14

realistic calculations of the EoS of NeuM have been made, and, while they all agree fairly closely at nuclear and sub-nuclear densities, at the much higher densities that can be encountered towards the center of neutron stars they differ greatly in their stiffness, and there are very few data, either observational or experimental, to discriminate between the different possibilities. We therefore considered three different constraining EoSs of NeuM, as follows. The softest is the one that we label FP [23] in Ref. [4], the one of intermediate stiffness is the “A18 + δv + UIX*” EoS [24], which we label as APR, while our stiffest constraining EoS is the one labeled “V18” in Ref. [25], which we refer to as LS2 in Ref. [4].

In constraining our forces to the EoS of NeuM we paid particular attention to the high densities appropriate to neutron-star cores. At the same time all of the models of this paper were fitted to one value or another of the symmetry coefficient J in the range 29 to 32 MeV. That we were able to adjust the symmetry energy at supernuclear densities more or less independently of the symmetry energy at nuclear densities is a consequence of the high flexibility of the 16-parameter Skyrme force that we have taken.

2.1 The 2010 Models

The three density functionals of Ref. [4], BSk19, BSk20 and BSk21, were constrained by the FP, APR and LS2 EoSs of NeuM, respectively, i.e., in ascending order of high-density stiffness. All had the value of 30 MeV for the symmetry coefficient J imposed on them, and all of them were fitted to the 2149 measured masses of nuclei with N and $Z \geq 8$ given in the 2003 AME [26], that being the latest available at the time. The rms deviation of these mass fits was 0.58 MeV in all three cases. We showed in Fig. 1 of Ref. [4] how well each of the three models reproduces its realistic “target” EoS of NeuM.

One might expect that the stiffer the constraining EoS the greater the maximum neutron-star mass that can be supported, and this was indeed found to be the case [27] on solving the Tolman-Oppenheimer-Volkoff (TOV) equations [28, 29] and imposing causality, as can be seen in the first three lines of Table 1. As a matter of fact, the maximum neutron-star masses thus obtained are very close to

those found with the corresponding constraining microscopic equation of state of NeuM. After the publication of our 2010 paper [4] the neutron stars PSR J1614–2230 and PSR J0348+0432 were shown to have masses of $1.97 \pm 0.04 \mathcal{M}_\odot$ [30] and $2.01 \pm 0.04 \mathcal{M}_\odot$ [31], respectively. This means that the neutron-star matter EoS obtained with BSk19 is definitely too soft, and it must be discarded. This does not necessarily imply that the NeuM EoS has to be much stiffer than that of FP, because the core of neutron stars may contain non-nucleonic particles (see, e.g., Ref. [32]); we do not consider this possibility any further in this paper.

2.2 The 2013 Models

In refitting to the 2353 measured masses of nuclei having N and $Z \geq 8$ in the 2012 AME [1] we took the opportunity of imposing different values of the symmetry coefficient J on our fits. We generated in all five new parameter sets, BSk22 to BSk26, along with the corresponding mass tables, labeled HFB-22 to HFB-26, respectively [20]. BSk22 to BSk25 were fitted to $J = 32, 31, 30$ and 29 MeV, respectively, and were all constrained to LS2, while BSk26 was also fitted to $J = 30$ MeV but under the APR constraint.

The rms and mean (data - theory) values of the deviations between the measured masses and the predictions for the five new models are given in the first and second lines, respectively, of Table 2. The next two lines of this table show the corresponding deviations for the subset consisting of the most neutron-rich measured nuclei, here taken as those with a neutron separation energy $S_n \leq 5.0$ MeV (there are 257 nuclei in this subset). All five models display, not surprisingly, some deterioration as we move into the neutron-rich region. From the first line we see that the parameter sets BSk24 ($J = 30$ MeV) and BSk25 ($J = 29$ MeV) give the best global fits of all the new models, and in fact are better than any of our previous models. However, line 3 of Table 2 shows that the deterioration of BSk25 on moving into the neutron-rich region is much stronger than for BSk24: for all the other models the performance in the neutron-rich region correlates fairly well with the global performance. Thus the apparent high performance of this model in the global fit should be interpreted with caution; other defects of model BSk25 are discussed in Ref. [20]. Looking at BSk22 and BSk23, we see from both lines 1 and 3 that $J = 31$ MeV works less well than either 29 or 30 MeV, while $J = 32$ MeV is still more strongly disfavoured.

Comparing BSk24 and BSk26 shows that for $J = 30$ MeV the high-density LS2 constraint (BSk24) gives slightly better fits than APR (BSk26). It must be stressed, however, that this discrimination in favour of LS2 as the constraining EoS of NeuM relates only to nuclear and subnuclear densities. In particular, we should not conclude that nuclear masses are telling us something about the EoS of NeuM at the higher densities found in neutron-star cores, since it is conceivable that our 16-parameter Skyrme form could be generalized still further in such a way that the

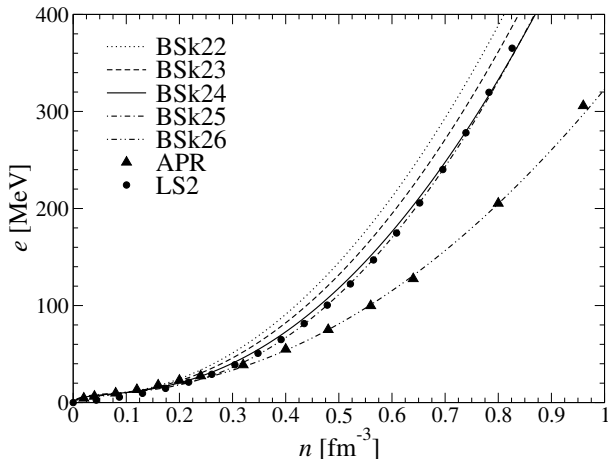


Fig. 1. Zero-temperature EoSs for neutron matter with models BSk22-26. APR is the realistic EoS “A18 + δv + UIX*” in Ref. [24]. LS2 is the realistic EoS “V18” in Ref. [25].

EoS at high densities was changed without affecting the fit to nuclear masses.

Overall, the clearest conclusion that can be drawn from Table 2 is that model BSk22 is the worst performing of all our models, ruling out $J = 32$ MeV. There are also very strong indications that $J = 29$ or 30 MeV (the latter in both its LS2 and APR forms) are to be preferred to $J = 31$ MeV, although we have expressed some concerns with regards to $J = 29$ MeV, i.e., to BSk25. In any case, it will be seen that the HFB models favour a value of J considerably higher than what we found from the simple drop model of Eq. (1), illustrating thereby the importance of using a model that takes account of the fine details on nuclear structure.

In Fig. 1 we show the neutron-matter EoSs of our five models; it will be seen how well they fit their “target” EoSs. Calculating symmetric INM for the five models enables us to calculate the symmetry energy $S_2(n)$, as given by Eq. (6). We show in Fig. 2 the variation of $S_2(n)$ with density for models BSk22 ($J = 32$ MeV, constrained by LS2), BSk24 ($J = 30$ MeV, constrained by LS2) and BSk26 ($J = 30$ MeV, constrained by APR); with this choice of models we are able to sample the influence of both the symmetry energy at nuclear densities and the high-density behavior of NeuM. We do not show the corresponding curves for symmetric INM, but they are all remarkably similar (see the discussion of this point in Section IIIA of Ref. [4]).

Neutron skins. The most extensive set of measurements of neutron-skin thicknesses using a given method is that of Ref. [33], which used antiproton scattering to measure 26 nuclei. In Table 3 we show the rms deviations σ_{rms} between our models and experiment, the mean deviations $\bar{\epsilon}$ and the model error σ_{mod} of Möller and Nix [34]. This last quantity provides a more reliable method of assessing the relative performance of different models, especially when the experimental errors are large, as in the present case. In the first three columns of this table we show the results for the full set of 26 nuclei, while in the next three columns

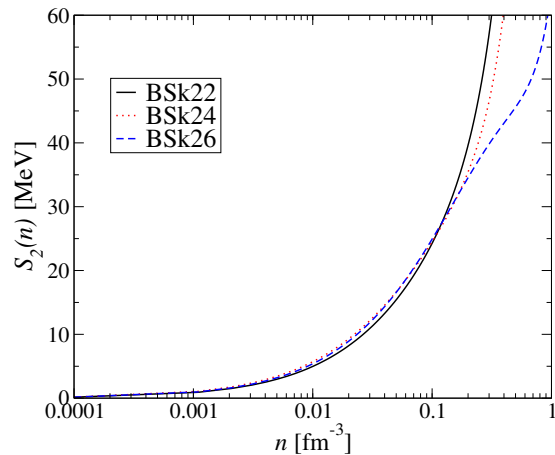


Fig. 2. Symmetry energy $S_2(n)$ for models BSk22, BSk24 and BSk26.

Table 4. J and higher-order symmetry coefficients for the 2013 models.

	BSk22	BSk23	BSk24	BSk25	BSk26
J [MeV]	32.0	31.0	30.0	29.0	30.0
L [MeV]	68.5	57.8	46.4	36.9	37.5
K_{sym} [MeV]	13.0	-11.3	-37.6	-28.5	-135.6
K' [MeV]	275.5	275.0	274.5	316.5	282.9

we consider only the 10 nuclei for which the experimental errors are 0.04 fm or less. We see that all three deviations, for both the complete set of data and the subset, show that models BSk24 and BSk26 are in better agreement with experiment than are the other models, thereby supporting the conclusion drawn from masses favoring $J = 30$ MeV.

Correlations between J and higher-order symmetry coefficients. In Table 4 we show for each of our 2013 models the values of J and the higher-order symmetry coefficients, L and K_{sym} defined in Eq. (5b). Although we have concluded that J must have a value close to 29 or 30 MeV, with 32 MeV definitely excluded, it is still of interest to see what happens to L and K_{sym} when we vary J over the full range of 29 to 32 MeV. Table 4 shows that in our models L is strongly correlated with J , confirming what was first established at least 35 years ago [35]. In fact, when plotted in the $J - L$ plane all our models fall within the elliptical region labeled “Nuclear masses” in Fig. 12 of Ref. [19]. Actually, if we compare the L -values for models BSk24 and BSk26, both of which have $J = 30$ MeV, we see that there is some dependence on the constraining EoS, the softer EoS leading, not surprisingly, to a lower value of L .

The influence of the constraining EoS is seen to be much stronger in the case of K_{sym} , the correlation with J (or L) being quite weak; clearly, a determination of L will not suffice to determine K_{sym} , contrary to the assertion of Ref. [36]. This apparent correlation between K_{sym} and the constraining EoS of NeuM might tempt one to conclude

Table 2. Rms (σ) and mean ($\bar{\epsilon}$) deviations between data and predictions for the 2013 models. The first pair of lines refers to all the 2353 measured masses M that were fitted [1], and the second pair to the masses M_{nr} of the subset of 257 neutron-rich nuclei ($S_n \leq 5.0$ MeV).

	HFB-22	HFB-23	HFB-24	HFB-25	HFB-26
$\sigma(M)$ [MeV]	0.629	0.569	0.549	0.544	0.564
$\bar{\epsilon}(M)$ [MeV]	-0.043	-0.022	-0.012	0.008	0.006
$\sigma(M_{nr})$ [MeV]	0.817	0.721	0.702	0.791	0.749
$\bar{\epsilon}(M_{nr})$ [MeV]	0.221	0.090	0.011	0.023	0.230

Table 3. Rms, mean and model deviations between 2013 models and the neutron-skin thickness measurements of Ref. [33]. The first three columns relate to the complete set of 26 nuclei, the last three columns to the set of 10 nuclei with the lowest experimental error.

	σ_{rms} (26)	$\bar{\epsilon}$ (26)	σ_{mod} (26)	σ_{rms} (10)	$\bar{\epsilon}$ (10)	σ_{mod} (10)
BSk22	0.0495	-0.0266	0.0205	0.0429	-0.030	0.0244
BSk23	0.0447	-0.0142	0.0090	0.0342	-0.017	0.0128
BSk24	0.0437	-0.0031	0.0047	0.0270	-0.0030	0.0087
BSk25	0.0469	0.0088	0.0170	0.0277	0.011	0.0194
BSk26	0.0415	-0.0038	0.0044	0.0265	-0.0040	0.0084

that a measurement of K_{sym} will suffice to determine the high-density EoS of NeuM. Once again, however, we must realize that our 16-parameter Skyrme form could be generalized still further, making it possible to change the EoS at high densities without affecting K_{sym} .

Extrapolation of masses far from the stability line. We show in Fig. 3, for all the nearly 8500 nuclei with $8 \leq Z \leq 110$ lying between the proton and neutron drip lines, the deviations between mass models HFB-22 ($J = 32$ MeV) and HFB-24 ($J = 30$ MeV). Discrepancies of up to 10 MeV will be seen, and it is noteworthy that the lower the J -value the larger the masses predicted far from the stability line. This behaviour is somewhat counter-intuitive, but it is by no means peculiar to the present forces, having been remarked before [37]. The explanation can be found in Fig. 2, where it will be seen that the average value of the symmetry energy over the nuclear volume is smaller the greater J (this argument remains valid whether one takes S_1 or S_2). In the liquid-drop model this average symmetry energy corresponds to the coefficient $(J + a_{ss}A^{-1/3})$ of the I^2 term in Eq. (1), so that we should expect a strong anticorrelation between J and the surface-symmetry coefficient a_{ss} . This we have verified to be the case by fitting the mass data for different fixed values of J , and we have found in fact that $(J + a_{ss}A^{-1/3})$ decreases with increasing values of J for all realistic values of A .

Neutron drip lines. We show in Fig. 4 the neutron drip lines for mass models HFB-22, HFB-24 and HFB-26. Recalling that the neutron drip line represents for each value of Z the lowest value of N for which the neutron separation energy S_n vanishes, it will be understood that the position of the drip line for any given model will be highly sensitive to the small random numerical errors that are inevitable in computing. Thus in calculating the drip lines we first apply the noise filter described in the Appendix,

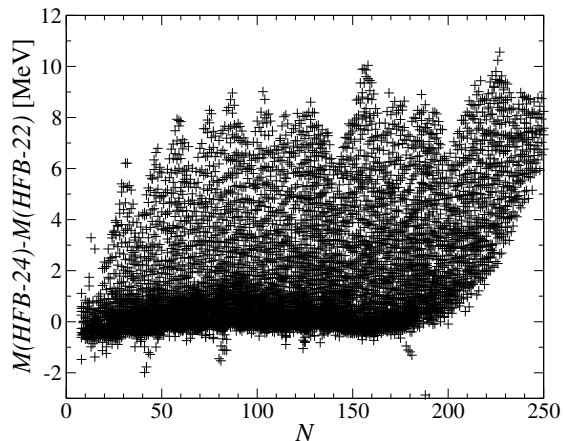


Fig. 3. Differences between HFB-22 and HFB-24 mass predictions for all nuclei between the drip lines.

denoting the model thereby generated by HFB-22*, etc. (nowhere else in this paper, or in any other that we have published so far, do we use these noise-filtered models).

Given the sensitivity to J of the masses of nuclei far from the stability line seen in Fig. 3, it is somewhat surprising that the different drip lines shown in Fig. 4 lie so close to each other. The reason is that the S_n of these nuclei are much less sensitive to J than are the masses.

3 Implications of HFB models for neutron stars

We have calculated the composition and EoS in all three regions of neutron stars (outer crust, inner crust and core) for the three typical 2013 models: BSk22 ($J = 32$ MeV,

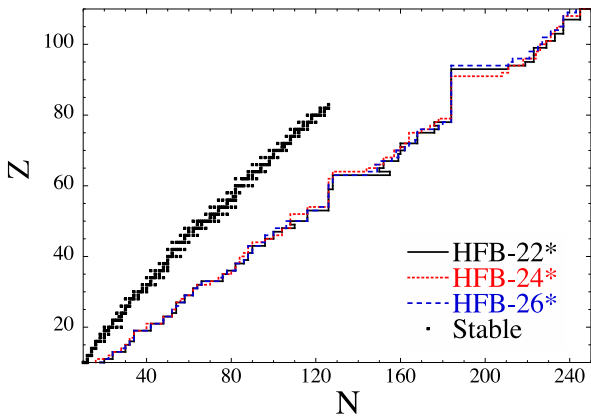


Fig. 4. Neutron drip lines for models HFB-22, HFB-24 and HFB-26.

constrained by LS2), BSk24 ($J = 30$ MeV, constrained by LS2) and BSk26 ($J = 30$ MeV, constrained by APR). The outer crust is calculated as in Ref. [7], and the inner crust as in Ref. [17], except that we now take into account proton pairing correlations in the BCS approximation along the lines of Ref. [18]. The calculation of the neutron-star matter of the core is, in view of the homogeneity, essentially exact: analytic expressions for both the nuclear and leptonic (electrons and muons) contributions are given in Ref. [21], and minimization with respect to the proton fraction Y_p and the muonic fraction of the leptons can be carried through to any required degree of accuracy.

The variation of Y_p with density over the entire star that we found for the three models is shown in Fig. 5, where the boundaries between the three regions are indicated. As we move below the surface the energy of the degenerate electrons dominates and the protons begin to capture electrons, i.e., Y_p decreases. However, at some point in the core the process is reversed and Y_p begins to increase with increasing density. That is, the neutronisation of protons gives way to the protonisation of neutrons through beta decay, because the nuclear symmetry energy rises so rapidly that it dominates the degenerate electrons. All three models behave very similarly as far as Y_p is concerned, but differences can be discerned in the higher density range of Fig. 5, and in fact they are seen to be correlated with the differences in the symmetry energy shown in Fig. 2.

The proton fraction Y_p is not the only composition variable of interest. For many purposes it is important to know the values of the proton number Z for the nuclei of the outer crust; we do not show them here, but we will publish them elsewhere. The situation concerning the Z -values of the clusters in the Wigner-Seitz cells of the inner crust is very simple: we have $Z = 40$ throughout the inner crust for all models, except for BSk22, where $Z = 20$ is favoured for densities higher than 0.035 nucleons per cubic fermis. (Actually, the existence of strong shell effects for $Z = 20$ and 40 is evident throughout the inner crust; the absence of $Z = 28$ might be taken as an indication of a suppression of the spin-orbit coupling.)

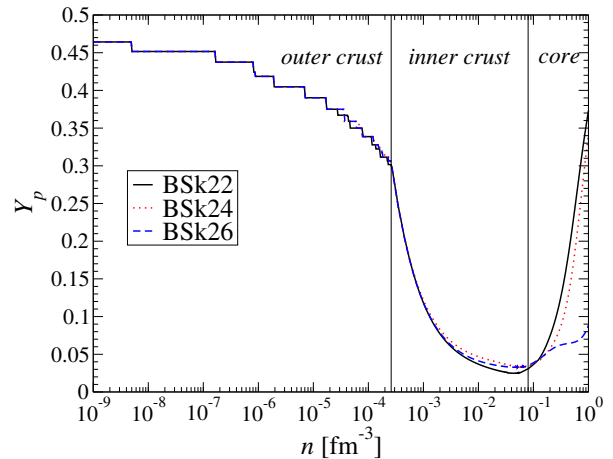


Fig. 5. Proton fraction Y_p as a function of mean local density in neutron stars for models BSk22, BSk24 and BSk26.

Maximum mass. Using the EoS that we have calculated, we solve the TOV equations to obtain the maximum mass of non-rotating stars for each of the five new density functionals of 2013, and can thereby complete Table 1. The numerical calculations have been done using the LORENE library (<http://www.lorene.obspm.fr>, see also Ref. [38]). We see that all our new models are compatible with the existence of the massive neutron stars PSR J1614–2230 and PSR J0348+0432. It turns out that the maximum mass is essentially the same for all models constrained by the same EoS of NeuM, and, in particular, seems to be independent of the symmetry energy.

Mass-radius relation. In a similar way we calculated the mass-radius relation for non-rotating stars with each of the models BSk22, BSk24 and BSk26. Our results are compared with the constraints obtained from astrophysical observations of three X-ray bursters of type I with photospheric radius expansion, and three transient low-mass X-ray binaries in globular clusters [39]. It will be seen in Fig. 6 that model BSk22 fails completely this test, BSk24 is at the limit of acceptability, while BSk26 is highly satisfactory. Thus, once again, we have support for preferring $J = 30$ MeV over 32 MeV, while the APR EoS of NeuM seems to be somewhat favoured over the stiffer LS2 EoS.

Direct Urca. The density above which the direct Urca process is allowed is indicated in Table 5, as well as the corresponding neutron-star mass for models BSk22, BSk24 and BSk26. All models predict the onset of the direct Urca process at high enough densities. But for the model BSk26, this process occurs at densities exceeding the central density in the most massive stable neutron star. On the other hand, the pulsar in CTA1, the transiently accreting millisecond pulsar SAX J1808.4–3658 and the soft X-ray transient 1H 1905+000 appear to be too cold, thus suggesting that these neutron stars cool very fast via the direct Urca process [40, 41, 42]. Moreover, the low luminosity from several young supernova remnants likely to contain a still unobserved neutron star [43, 44] provide further evidence for a direct Urca process [42, 45]. If this interpretation is correct, model BSk26 would be ruled out.

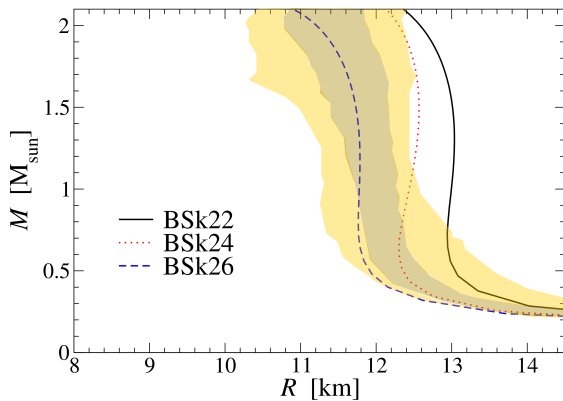


Fig. 6. Mass-radius relation of neutron stars for models BSk22, BSk24 and BSk26. The dark (light) shaded regions correspond to the 1- σ (2- σ) probability distributions implied by observation, as shown in the upper right panel of Fig. 9 of Ref. [39].

Table 5. Threshold density for the direct Urca process to occur, and corresponding neutron-star mass for models BSk22, BSk24 and BSk26.

	n_{du}	$\mathcal{M}_{du}/\mathcal{M}_{\odot}$
BSk22	0.33	1.14
BSk24	0.45	1.59
BSk26	1.46	-

In addition, the model BSk22 is found to be incompatible with the constraint of Klähn et al. [46] that no direct Urca process should occur in neutron stars with typical masses in the range $\mathcal{M} \sim 1 - 1.5 \mathcal{M}_{\odot}$, leaving thereby BSk24 as the only model consistent with both constraints.

We do not show here the EoSs that we have calculated and that are implicit in all the results of this section, but will publish them elsewhere.

4 Conclusions

We have described the main features of our most recent HFB mass models, which have been fitted to the mass data of the 2012 AME. Our preferred model, HFB-24, fits the 2353 measured masses of nuclei with N and $Z \geq 8$ with an rms deviation under 0.55 MeV. A symmetry coefficient of $J = 30$ MeV is favoured, with strong indications against a value of 32 MeV.

These mass models, taken with their underlying functionals, permit a unified treatment of all regions of neutron stars. We have calculated with each of our models the composition and EoS of neutron stars. Solving then the TOV equations we were able to calculate the mass-radius relation for each model, which, when compared with the observational constraints, strongly favours $J = 30$ MeV over 32 MeV. Moreover, all our models lead to maximum masses greater than the heaviest observed neutron stars.

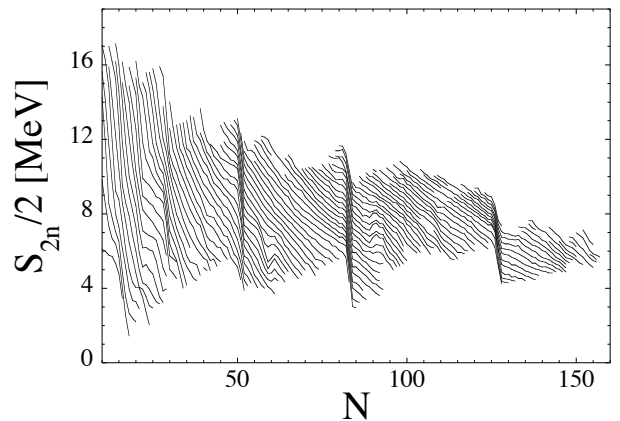


Fig. 7. Two-neutron separation energies for all isotopic chains with known masses

This work was financially supported by the F.R.S.-FNRS (Belgium) and the NSERC (Canada).

A Noise-filtering of the calculated model masses

In Fig. 7 we show the experimental values [1] of the two-neutron separation energy S_{2n} and in Fig. 8 the calculated (HFB-24) values. It will be seen in this latter figure that despite the excellent global fit to the mass data there are many small irregularities in the calculated masses, with the different isotopic curves sometimes touching and even crossing each other, while the experimental curves (Fig. 7) are much smoother and more regularly spaced. This spurious structure is a noise that inevitably occurs in the extensive numerical procedures involved in solving the HFB equations.

There is, of course, no unambiguous way to filter out this noise, but here we describe a procedure that we have developed on the basis of the 21-nucleus variation of the Garvey-Kelson relations [47], abbreviated here as 21GK, shown by Barea *et al.* [48] to be well satisfied by the mass data of the 2003 AME [26], the rms deviation for all nuclei with $A \geq 16$ being 0.087 MeV. The degree of smoothness displayed by the 21GK masses is thus much closer to what is seen in the data than in the HFB results.

Our method proceeds reiteratively, with the mass of the nucleus (Z, N) after the i 'th iteration being expressed

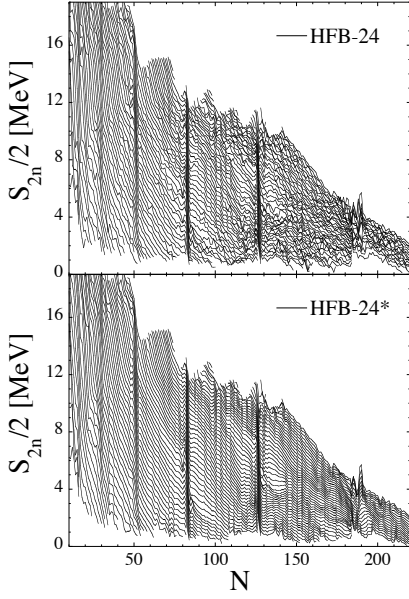


Fig. 8. $S_{2n}/2$ surfaces for HFB24 mass table before (upper panel) and after (lower panel) filtering the masses by the “21GK” method described in the text.

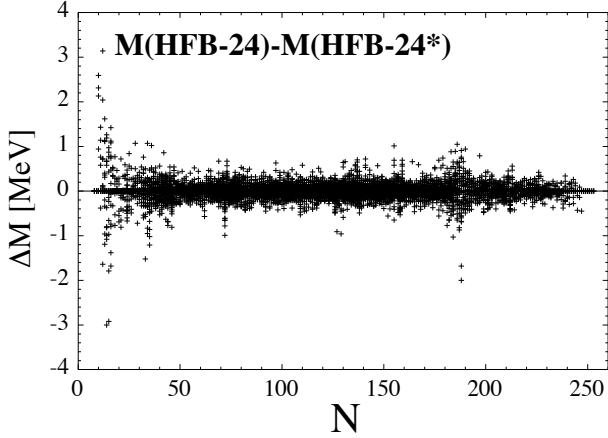


Fig. 9. Mass differences between the noise-filtered version of the HFB-24 model and the original version, as a function of neutron number N for the 8509 nuclei included in the mass table.

as

$$\begin{aligned}
 M_i(Z, N) = & \\
 & \frac{1}{12} [M_{i-1}(Z+2, N-2) + M_{i-1}(Z+2, N+2) \\
 & + M_i(Z-2, N-2) + M_i(Z-2, N+2) \\
 & - 2 M_{i-1}(Z+2, N-1) - 2 M_{i-1}(Z+2, N+1) \\
 & - 2 M_{i-1}(Z+1, N-2) - 2 M_{i-1}(Z+1, N+2) \\
 & - 2 M_i(Z-1, N-2) - 2 M_i(Z-1, N+2) \\
 & - 2 M_i(Z-2, N-1) - 2 M_i(Z-2, N+1) \\
 & + 2 M_{i-1}(Z, N+2) + 2 M_{i-1}(Z+2, N) \\
 & + 2 M_i(Z, N-2) + 2 M_i(Z-2, N) \\
 & + 4 M_{i-1}(Z, N+1) + 4 M_{i-1}(Z+1, N) \\
 & + 4 M_i(Z, N-1) + 4 M_i(Z-1, N)], \quad (\text{A1})
 \end{aligned}$$

where we complete one isotope chain at a time, beginning with the lowest value of Z , before passing to the next value of Z ; for each chain we begin with the lowest value of N . Thus to estimate the mass $M(Z_0, N_0)$, the masses entering the right-hand side of Eq. (A1) correspond to the new iteration for $Z < Z_0$ and also for $Z = Z_0$ provided $N < N_0$; otherwise we take the previous iteration. The initial iteration, $i = 0$, corresponds to the original HFB value. We emphasize that this procedure is not applied to nuclei if both the neutron and proton number differ by less than two units from a magic number, thereby keeping the sharp shell closure predicted by the HFB calculations and seen experimentally. This procedure can be applied only to nuclei for which the mass of the 20 neighbouring nuclei is included in the mass table (see Eq. A1). We iterate 5 times, in order to achieve some degree of convergence. The resulting $S_{2n}/2$ mass surface for all isotope chains with model HFB-24 is shown in the lower panel of Fig. 8. The success of our procedure becomes apparent on comparing with the same quantities for the original HFB-24 model, before filtering. It will be seen that there has been a significant reduction in the noise level.

Fig. 9 shows for all 8509 nuclei included in the HFB-24 mass table the actual shift in the calculated masses brought about by our noise-filtering procedure. The rms value of the shift over all three models is 0.20 MeV, although for specific cases (notably light nuclei) the shift can amount to more than 1 MeV.

As for the impact of our procedure on the experimentally known nuclei, the rms deviation for all 2353 known nuclei increases by no more than 4 keV with respect to the original HFB table, and for the 257 most neutron-rich nuclei with $S_n \leq 5$ MeV an improvement of 7 keV is found. Not surprisingly, there is a slight improvement by some 20 keV in the rms deviations of the differential quantities S_n and Q_β .

We stress that we are not using the Garvey-Kelson method [47] in its traditional role as a means of extrapolating masses from known to unknown nuclei: to do so would have led to enormous deviations from the HFB results. Rather, this extrapolation is performed at the level of the original HFB calculations, once the forces have been obtained. In other words, the Garvey-Kelson method, in the form of Eq. (A1), is applied to all the HFB-calculated masses in the same way, regardless of whether they refer to measured or unmeasured nuclei. Thus the HFB result for *every* nucleus leaves its imprint on the final noise-filtered result.

References

1. G. Audi, M. Wang, A.H. Wapstra, F.G. Kondev, M. MacCormick, X. Xu, and B. Pfeiffer, *Chinese Physics C* **36** (2012), 1287.
2. J. M. Pearson, *Hyperfine Interac.* **132** (2001), 59
3. N. Chamel and P. Haensel, “Physics of Neutron Star Crusts”, *Living Rev. Relativity* **11** (2008), 10. <http://www.livingreviews.org/lrr-2008-10>

4. S. Goriely, N. Chamel, and J. M. Pearson, *Phys. Rev. C* **82**, 035804 (2010).
5. M. B. Tsang et al., *Phys. Rev. C* **86** (2012), 015803.
6. S. B. Rüster, M. Hempel, and J. Schaffner-Bielich, *Phys. Rev. C* **73**, 035804 (2006).
7. J. M. Pearson, S. Goriely, and N. Chamel, *Phys. Rev. C* **83**(2011) 065810.
8. R. N. Wolf, D. Beck, K. Blaum, Ch. Böhm, Ch. Borgmann, M. Breitenfeldt, N. Chamel, S. Goriely, F. Herfurth, M. Kowalska, S. Kreim, D. Lunney, V. Manea, E. Minaya Ramirez, S. Naimi, D. Neidherr, M. Rosenbusch, L. Schweikhard, J. Stanja, F. Wienholtz, K. Zuber, *Phys. Rev. Lett.* **110** (2013) 041101.
9. J. W. Negele and D. Vautherin, *Nucl. Phys.* **A207** (1973) 298.
10. M. Baldo, E. E. Saperstein, S. V. Tolokonnikov, *The European Physical Journal A* **32** (2007) 97.
11. F. Grill, J. Margueron, N. Sandulescu, *Phys. Rev. C* **84** (2011) 065801.
12. N. Chamel, S. Naimi, E. Khan, and J. Margueron, *Phys. Rev. C* **75**(2007) 055806.
13. P. Magierski and P.-H. Heenen, *Phys. Rev. C* **65** (2002) 045804.
14. P. Gögelein, E. N. E. van Dalen, C. Fuchs, H. Müther, *Phys. Rev. C* **77**(2008) 025802.
15. W.G. Newton and J.R. Stone, *Phys. Rev. C* **79**(2009) 055801.
16. M. Onsi, A. K. Dutta, H. Chatri, S. Goriely, N. Chamel, and J. M. Pearson, *Phys. Rev. C* **77** (2008) 065805.
17. J. M. Pearson, N. Chamel, S. Goriely, C. Ducoin, *Phys. Rev. C* **85** (2012) 065803.
18. J. M. Pearson, Y. Aboussir, A. K. Dutta, R. C. Nayak, M. Farine, and F. Tondeur, *Nucl. Phys.* **A528**, 1 (1991).
19. J. M. Lattimer, *Annu. Rev. Nucl. Part. Sci.* **62** (2012) 485.
20. S. Goriely, N. Chamel, and J. M. Pearson, submitted to *Phys. Rev. C* (2013).
21. N. Chamel, S. Goriely, and J. M. Pearson, *Phys. Rev. C* **80** (2009) 065804.
22. N. Chamel and S. Goriely, *Phys. Rev. C* **82**, 045804 (2010).
23. B. Friedman and V. R. Pandharipande, *Nucl. Phys.* **A361** (1981) 502.
24. A. Akmal, V. R. Pandharipande, and D. G. Ravenhall, *Phys. Rev. C* **58** (1998) 1804.
25. Z. H. Li and H.-J. Schulze, *Phys. Rev. C* **78** (2008) 028801.
26. G. Audi, A.H. Wapstra, and C. Thibault, *Nucl. Phys.* **A729** (2003) 337.
27. N. Chamel, A. F. Fantina, J. M. Pearson, and S. Goriely, *Phys. Rev. C* **84** (2011) 062802(R).
28. R. C. Tolman, *Phys. Rev.* **55** (1939) 364.
29. J. R. Oppenheimer and G. M. Volkoff, *Phys. Rev.* **55** (1939) 374.
30. P. B. Demorest, T. Pennucci, S. M. Ransom, M. S. E. Roberts, J. W. T. Hessels, *Nature* **467** (2010) 1081.
31. J. Antoniadis, P. C. C. Freire, N. Wex, T. M. Tauris, R. S. Lynch, M. H. van Kerkwijk, M. Kramer, C. Bassa, V. S. Dhillon, T. Driebe, J. W. T. Hessels, V. M. Kaspi, V. I. Kondratiev, N. Langer, T. R. Marsh, M. A. McLaughlin, T. T. Pennucci, S. M. Ransom, I. H. Stairs, J. van Leeuwen, J. P. W. Verbiest, D. G. Whelan, *Science* **340** (2013) 1233232.
32. N. Chamel, A. F. Fantina, J.M. Pearson, S. Goriely, *Astron. Astrophys.* **553** (2013) A22.
33. J. Jastrzębski, A. Trzcńska, P. Lubiński, B. Cios, F. J. Hartmann, T. von Egidy, and S. Wycech, *Int. Journ. Mod. Phys. E* **13** (2004) 343.
34. P. Möller and J. R. Nix, *At. Data Nucl. Data Tables* **39** (1988) 213.
35. M. Farine, J. M. Pearson, and B. Rouben, *Nucl. Phys.* **A304** (1978) 317.
36. J. Dong, W. Zuo, J. Gu, and U. Lombardo, *Phys. Rev. C* **85** (2012) 034308.
37. S. Goriely, M. Samyn, J. M. Pearson, and M. Onsi, *Nucl. Phys.* **A750** (2005) 425.
38. E. Gourgoulhon, lectures given at the Compstar 2010 School, arXiv:1003.5015v1
39. A. W. Steiner, J. M. Lattimer, E. F. Brown, *Astrophys. J.* **722**, 33 (2010).
40. P. G. Jonker, D. Steeghs, D. Chakrabarty, A. M. Juett, *Astrophys. J.* **665**, L147 (2007).
41. C. O. Heinke, P. G. Jonker, R. Wijnands, C. J. Deloye, R. E. Taam, *Astrophys. J.* **691**, 1035 (2009).
42. D. Page, J. M. Lattimer, M. Prakash, A. W. Steiner, *Astrophys. J.* **707**, 1131 (2009).
43. D. L. Kaplan, D. A. Frail, B. M. Gaensler, et al. *Astrophys. J. Suppl.* **153**, 269 (2004).
44. D. L. Kaplan, B. M. Gaensler, S. -R. Kulkarni, P. O. Slane, *Astrophys. J. Suppl.* **163**, 344 (2006).
45. P. S. Shternin, D. G. Yakovlev, *Astronomy Letters* **34**, 675 (2008).
46. T. Klähn, D. Blaschke, S. Typel, et al., *Phys. Rev. C* **74**, 035802 (2006).
47. G.T. Garvey, W.J. Gerace, R.L. Jaffe, I. Talmi, and I. Kelson, *Rev. Mod. Phys.* **41**, S1 (1969).
48. J. Barea, A. Frank, J.G. Hirsch, P. Van Isacker, S. Pittel, and V. Velazquez, *Phys. Rev. C* **77**, 041304(R) (2008).